Biophysical Journal
Article

Biophysical Society

Simultaneous Release of Multiple Vesicles from Rods Involves Synaptic Ribbons and Syntaxin 3B

Cassandra L. Hays,[1,2] Justin J. Grassmeyer,[2,3] Xiangyi Wen,[2,4] Roger Janz,[5,6] Ruth Heidelberger,[5,6] and Wallace B. Thoreson[2,3,*]

[1]Department of Cellular and Integrative Physiology, [2]Department of Ophthalmology and Visual Sciences, Truhlsen Eye Institute, and [3]Department of Pharmacology and Experimental Neuroscience, University of Nebraska Medical Center, Omaha, Nebraska; [4]West China Hospital, Sichuan University, Chengdu, Sichuan, P.R. China; [5]Department of Neurobiology and Anatomy, McGovern Medical School, University of Texas Health Science Center at Houston, Houston, Texas; and [6]The University of Texas MD Anderson Cancer Center University of Texas Health Graduate School of Biomedical Sciences, Houston, Texas

ABSTRACT First proposed as a specialized mode of release at sensory neurons possessing ribbon synapses, multivesicular release has since been described throughout the central nervous system. Many aspects of multivesicular release remain poorly understood. We explored mechanisms underlying simultaneous multivesicular release at ribbon synapses in salamander retinal rod photoreceptors. We assessed spontaneous release presynaptically by recording glutamate transporter anion currents ($I_{A(glu)}$) in rods. Spontaneous $I_{A(glu)}$ events were correlated in amplitude and kinetics with simultaneously measured miniature excitatory postsynaptic currents in horizontal cells. Both measures indicated that a significant fraction of events is multiquantal, with an analysis of $I_{A(glu)}$ revealing that multivesicular release constitutes ~30% of spontaneous release events. $I_{A(glu)}$ charge transfer increased linearly with event amplitude showing that larger events involve greater glutamate release. The kinetics of large and small $I_{A(glu)}$ events were identical as were rise times of large and small miniature excitatory postsynaptic currents, indicating that the release of multiple vesicles during large events is highly synchronized. Effects of exogenous Ca^{2+} buffers suggested that multiquantal, but not uniquantal, release occurs preferentially near Ca^{2+} channels clustered beneath synaptic ribbons. Photoinactivation of ribbons reduced the frequency of spontaneous multiquantal events without affecting uniquantal release frequency, showing that spontaneous multiquantal release requires functional ribbons. Although both occur at ribbon-style active zones, the absence of cross-depletion indicates that evoked and spontaneous multiquantal release from ribbons involve different vesicle pools. Introducing an inhibitory peptide into rods to interfere with the SNARE protein, syntaxin 3B, selectively reduced multiquantal event frequency. These results support the hypothesis that simultaneous multiquantal release from rods arises from homotypic fusion among neighboring vesicles on ribbons and involves syntaxin 3B.

SIGNIFICANCE It is now recognized that many neurons and non-neuronal secretory cells can release multiple vesicles in response to stimulation. Among other properties, multivesicular release can improve the ability to encode the timing of events at neuronal synapses. Synaptic ribbons are protein structures in sensory neurons that tether vesicles near release sites and support multivesicular release. We studied mechanisms underlying spontaneous multiquantal release at large ribbon synapses of rod photoreceptor cells in salamander retina. Recording release events presynaptically in rods using glutamate transporter-associated anion currents, we found that multiquantal release involves homotypic fusion among vesicles on synaptic ribbons and believe it shows a novel role for the SNARE protein, syntaxin 3B, in promoting multiquantal release separate from its role in exocytosis.

INTRODUCTION

Early studies suggested that an action potential triggered fusion of only a single vesicle at most synapses, but there is increasing recognition that many synapses can release multiple vesicles (1). Synaptic ribbons in sensory neurons—protein structures that tether numerous vesicles near release sites—are specialized to support multivesicular release (1,2). Ribbon-bearing hair cells, retinal bipolar cells, and photoreceptor cells respond to sensory stimulation with graded changes in membrane potential that regulate the rate of ongoing vesicle release. While also

Submitted July 25, 2019, and accepted for publication October 3, 2019.

*Correspondence: wbthores@unmc.edu

Editor: Meyer Jackson.

https://doi.org/10.1016/j.bpj.2019.10.006

maintaining release almost indefinitely, ribbon synapses must be able to adjust release rapidly in response to changes in membrane potential. Release of a vesicle at synaptic ribbons in a number of different cell types, including rods, requires the opening of only a few nearby Ca^{2+} channels (3–6). Stimulating the opening of multiple Ca^{2+} channels with a rapid, strong depolarizing stimulus can thus trigger rapid fusion of multiple vesicles from the readily releasable pool docked at the base of a ribbon (3,7,8). However, even when Ca^{2+} channel openings are few and far between, one can observe spontaneous postsynaptic events that vary widely in amplitude. Although the amplitude of vesicle release events may also be shaped by the kinetics of vesicle pore opening (9,10), this suggests that even individual spontaneous events may involve the release of multiple vesicles (8,11–13). Multivesicular release may help ribbon synapses encode sensory information by regulating event amplitude as well as frequency (14).

A number of mechanisms have been proposed to account for multivesicular release. One is coincident fusion of individual vesicles located at different release sites along the base of the ribbon (12). One way this might occur is if Ca^{2+} ions entering Ca^{2+} channels beneath the ribbon spread far enough to trigger the fusion of multiple ribbon-associated vesicles (15,16). It has also been suggested that the amplification of Ca^{2+} influx by CICR from intracellular stores may promote multivesicular fusion in rods (17). Another potential mechanism for multivesicular release is homotypic fusion, in which neighboring vesicles fuse with one another either before or after fusion with the plasma membrane (18–22). Homotypic fusion of exocytotic vesicles is prominent in parotid and pancreatic acinar cells (21), immune cells (22–26), and pancreatic β cells (20,21,27). Vesicle-vesicle fusion has also been shown to increase quantal size at conventional neuronal synapses (28) and may occur at ribbon synapses in the retina (18,29,30).

Homotypic fusion among secretory vesicles depends on several SNARE and SNARE-associated proteins, including munc18-2 (31,32), munc13-4 (33,34), SNAP23 (35), and VAMP8 (36,37). In many secretory cells, vesicle-vesicle fusion involves syntaxin 3 (24,27,38). Similarly, retinal ribbon synapses of bipolar and photoreceptor cells use syntaxin 3B rather than the syntaxin 1 isoform used by most neurons (39,40). Although syntaxin is principally expressed on target membranes, it can also be found on vesicular membranes (41–43), including those of ribbon synapses (44). The close proximity of vesicles tethered next to one another on a synaptic ribbon (45) could potentially facilitate vesicle-vesicle fusion. It has therefore been hypothesized that syntaxin 3B might promote the formation of intervesicular SNARE complexes and homotypic fusion among neighboring vesicles on a ribbon (18).

We studied the frequency and mechanisms of simultaneous multiquantal release at ribbon synapses in rod photoreceptor cells of salamander retina. We measured release presynaptically by recording glutamate transporter anion currents ($I_{A(glu)}$) from rods. Excitatory amino acid transporters (EAATs) can be found in neurons and glial cells where they retrieve glutamate for terminating synaptic transmission and reuse (46–48). EAATs are electrogenic antiporters, exchanging glutamate, 3 Na^+, and 1 H^+ for 1 K^+ molecule; however, most of the EAAT current measured by whole cell voltage clamp is due to an uncoupled anion conductance (48). Although not directly coupled to glutamate transport, the EAAT anion current is linearly proportional to the number of glutamate ions released (49,50). The principal glutamate transporters in salamander rods are sEAAT2 and 5A; the latter exhibits a particularly large anion conductance (47,48). Measuring release presynaptically eliminates synapse-to-synapse variation in the number of glutamate receptors or differences in electrotonic distance among synapses that can contribute to quantal variability in postsynaptic measurement (51).

Our results show that ~30% of spontaneous release events in rods involve the simultaneous fusion of multiple vesicles. We found that simultaneous multiquantal fusion involves vesicles situated close to Ca^{2+} channels, is impaired by damage to ribbons, and is selectively reduced by interfering with syntaxin 3B. These results support the hypothesis that simultaneous multiquantal release at rod photoreceptor synapses is largely due to homotypic fusion of vesicles promoted by syntaxin 3B at synaptic ribbons.

METHODS

Retinal slices

Vertical slices were prepared from the retinae of aquatic tiger salamanders (*Ambystoma tigrinum*) as previously described (52). Animal husbandry and experimental procedures were approved by the University of Nebraska Medical Center's Institutional Animal Care and Use Committee. Salamanders of both sexes were housed in a water tank (4°C) on a 12:12-h light-dark cycle. Experiments were typically conducted 1–3 h after the beginning of subjective night. After brief submersion in 0.25 g/L MS222, salamanders were sacrificed by decapitation. After enucleating the eye, the cornea and iris were removed, and the resultant eyecup was cut into two or three pieces. One piece was then placed vitreal side down onto a nitrocellulose membrane. Under cold amphibian Ringer's solution, the retina was carefully isolated by removing the sclera, choroid, and pigment epithelium. A razor blade tissue slicer (Stoelting, Wood Dale, IL) was used to cut the retina into 125-μm slices. The thin slices of filter paper with attached retina were rotated 90° and anchored in the recording chamber by two strips of vacuum grease. Dissections were performed under cold amphibian Ringer's solution and room light. Retinal slices were visualized on an upright, fixed-stage microscope (Nikon E600FN, 60× 1.0 NA long working distance objective) and continuously superfused (1 mL/min) with an oxygenated amphibian saline solution containing (in mM) 116 NaCl, 2.5 KCl, 1.8 $CaCl_2$, 0.5 $MgCl_2$, 5 Glucose, and 10 HEPES (pH 7.8; room temperature).

Electrophysiology

Whole cell recordings were obtained from rods and horizontal cells in retinal slices. Patch-pipettes were crafted on a Narishige (Amityville,

NY) PP-830 vertical puller from borosilicate glass (1.2-mm outer diameter, 0.9-inner diameter with internal filament; World Precision Instruments, Sarasota, FL). Each had tip diameters of 1–2 μm and resistances of 5–15 MΩ. Recordings of $I_{A(glu)}$ from rod photoreceptors were obtained with a pipette solution using SCN^- as the principal anion to enhance $I_{A(glu)}$ (in mM): 90 KSCN, 10 TEA-Cl, 3.5 NaCl, 1 $MgCl_2$, 10 HEPES, 10 ATP-Mg, and 0.5 GTP-Na. Except for Ca^{2+} chelator experiments in which we used 0.05 mM EGTA or 10 mM 1,2-bis(o-aminophenoxy)ethane-N,N,N′,N′-tetraacetic acid (BAPTA), the solution also contained 5 mM EGTA. We did not correct for the liquid junction potential (LJP) calculated with PClamp (Axon Instruments, San Jose, CA) to be −4.5 mV. Recordings from horizontal cells used a pipette solution containing (in mM) the following: 90 CsGluconate, 10 TEA-Cl, 3.5 NaCl, 1 $MgCl_2$, 10 HEPES, 5 EGTA, 10 ATP-Mg, and 0.5 GTP-Na (18). The LJP for this solution was −12.2 mV. Rod recordings showed an average capacitance of 34.5 ± 3.0 pF, membrane resistance of 221.6 ± 24.8 MΩ, and series resistance of 26.5 ± 3.7 MΩ ($n = 16$).

For fluorophore-assisted laser inactivation (FALI) experiments described below, we included 80 μM fluorescein isothiocyanate (FITC)-conjugated RIBEYE-binding peptide or a scrambled version of the same peptide in the KSCN pipette solution, along with 3 mM reduced glutathione and 3 mM trolox as antioxidants (53). RIBEYE (or CtBP1) is a transcript variant of CtBP2 containing a ribbon-specific A domain and a B domain shared with CtBP2 (54). The FITC-conjugated peptide (FITC-Ahx-EQTVPLDLSKRDR) binds to a PXDLS sequence in CtBP2 (53). As a control, we used a scrambled version of the same peptide (FITC-Ahx-RTSPDKLVLDERQ).

To test a role for syntaxin 3B, we introduced 250 μM syntaxin 3B inhibitory peptide (stx3pep; RHKDIMRLESSIKELHDMFVDVA) or a scrambled version of the same peptide (RIALKDDVIHMRESVDHKSFMEL) into the pipette solution along with 1 mM reduced glutathione and 1 mM trolox (40).

Quantal analysis

Spontaneous rod $I_{A(glu)}$ events were recorded while holding rods at −70 mV. Trials were typically 180 s in duration. Individual $I_{A(glu)}$ events in rods and miniature EPSCs (mEPSCs) in horizontal cells were identified using the "event detection" function in Clampfit 10.4 with a template created from an average of 5–15 events from the same cell. During simultaneous recordings, rod $I_{A(glu)}$ and horizontal cell mEPSCs were considered to be coordinated if the onset of an $I_{A(glu)}$ event occurred within 10 ms of the beginning of an mEPSC. Amplitude histograms were constructed and fit with a multiple Gaussian function. Events within one SD of the mean of the first peak were considered "uniquantal," and remaining larger events were considered "multiquantal." Quantal content was calculated from weighted averages of the area under the curves from a multiple Gaussian fit (GraphPad Prism 4).

FALI

For FALI experiments, we introduced 80 μM FITC-conjugated RIBEYE-binding peptide or a scrambled version of the same peptide through the patch pipette into a rod. Immediately after rupture, we applied a 2-ms voltage step from −70 to −10 mV to evoke ribbon-mediated release and then recorded spontaneous events for 90 s while holding the rod at −70 mV. We followed this with a second 2-ms step and another 90-s measurement of spontaneous events. The 488-nm laser from the spinning disk confocal was then turned on for 60 s to bleach the FITC-conjugated peptide. After bleaching, we applied a 2-ms step followed by 90 s of recording spontaneous events and then a final 2-ms step. We analyzed trials with the RIBEYE-binding peptide in which discrete bright puncta were observed showing that the FITC-conjugated peptide had successfully bound to ribbons.

RESULTS

Spontaneous release events in rods

We studied vesicle fusion events in rods by recording presynaptic anion currents activated during glutamate uptake by EAATs in rod terminals. $I_{A(glu)}$ was enhanced by using the permeant SCN^- as the principal anion in the rod pipette solution. Although Cl^- ions are not directly involved in the process of glutamate transport, the amplitude of $I_{A(glu)}$ is linearly related to the number of glutamate molecules that are retrieved (49,50). As illustrated in Fig. 1 *A*, we observed

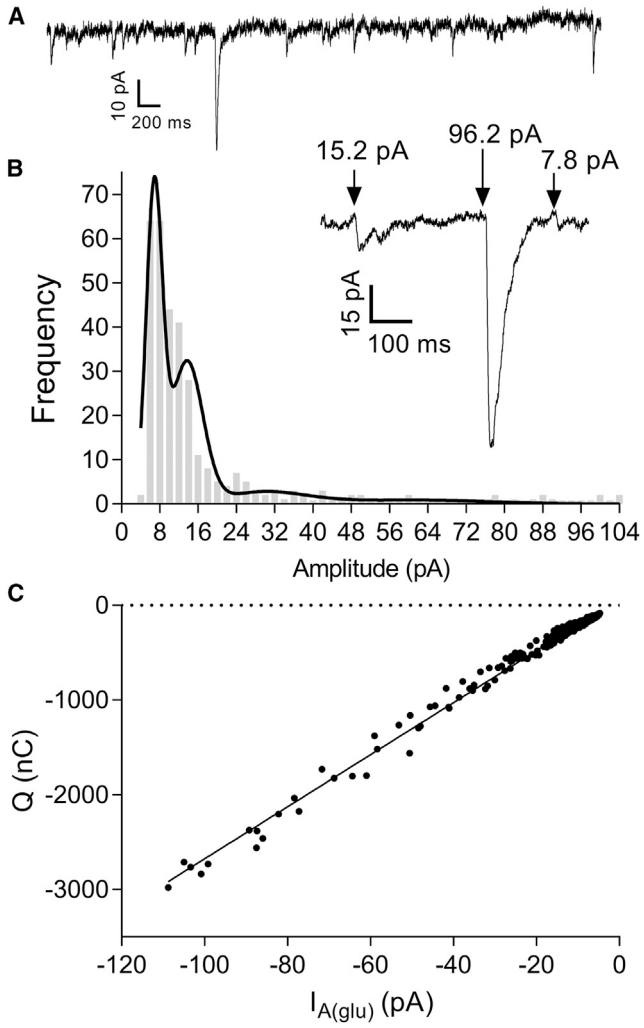

FIGURE 1 Amplitude characteristics of spontaneous $I_{A(glu)}$ events are consistent with multiquantal release. (*A*) Spontaneous multiquantal events were observed among many uniquantal events in rods voltage clamped at −70 mV. (*B*) Shown is a representative amplitude histogram of spontaneous rod $I_{A(glu)}$ events ($n = 325$) fit with a multiple Gaussian function. The inset shows a representative segment of the recording from which the histogram was derived. By assuming that the mean ± SD of the initial peak represents a single quantum, quantal content for this cell was calculated as a weighted average of the areas under the curve and found to be 1.69. (*C*) Amplitude of $I_{A(glu)}$ events ($n = 339$) was strongly correlated with event charge transfer (R = 0.99) with nonzero slope (F-test, $p < 0.0001$).

occasional large spontaneous $I_{A(glu)}$ events interspersed among more numerous smaller events in recordings from rods held under voltage-clamp control at −70 mV. Spontaneous $I_{A(glu)}$ events could be blocked with a glutamate transport inhibitor, threo-β-benzyloxyaspartic acid (11). Because light hyperpolarizes rods, voltage clamping them at −70 mV is functionally equivalent to strong light adaptation. Baseline noise during recordings of $I_{A(glu)}$ from rods voltage clamped at −70 mV could be further reduced by applying a bright background light to hyperpolarize neighboring rods and cones (data not shown). This suggests that glutamate released from photoreceptors in darkness can reach glutamate transporters of neighboring rods. To minimize the possible impact of release from neighbors, recordings were performed in strongly light-adapted preparations. The amplitude distributions of mEPSCs in horizontal cells did not differ significantly whether measured under scotopic or photopic conditions (8), suggesting that the relative frequency of multiquantal events is not significantly altered by light adaptation. Under these experimental conditions, the amplitude of spontaneous $I_{A(glu)}$ events in rods voltage clamped at −70 mV averaged 15.5 ± 1.61 pA (n = 16 rods, n = 49–1134 events/cell) with an average rise time of 13.8 ± 1.37 ms, half width of 9.65 ± 1.63 ms, and decay time of 23.2 ± 2.18 ms.

Fig. 1 *B* shows a representative amplitude histogram of spontaneous $I_{A(glu)}$ events. The inset shows a small section of the record from this cell illustrating both small and large events. Similar to amplitude histograms of mEPSCs (8,55,56), amplitude histograms of $I_{A(glu)}$ were skewed to the right (Fig. 1 *B*). And similar to monophasic excitatory postsynaptic currents (EPSCs) at other synapses (10,57), event amplitude and charge transfer of $I_{A(glu)}$ events increased linearly with one another indicating that larger amplitude events involve greater glutamate release (Fig. 1 *C*).

Binomial statistics predict that the distribution of event amplitudes should be fit by a sum of Gaussian functions with peaks that are integer multiples of one another (Fig. 1 *B*). The individual quantal amplitude obtained by fitting amplitude histograms with multiple Gaussians averaged 10.7 ± 2.02 pA compared with an overall mean amplitude of 15.5 ± 1.61 pA in the same cells. A multiple Gaussian function fit amplitude frequency distributions better than a single Gaussian ($p < 0.001$ for 7/8 cells; $p = 0.051$ for one cell). Quantal content was calculated from a weighted average of areas under the curves for each peak in the multiple Gaussian. From these multiple Gaussians, quantal content was estimated to be 1.53 ± 0.11 (n = 10) from rod $I_{A(glu)}$. We found a similar quantal content of 1.42 ± 0.09 (n = 8) from the amplitude of horizontal cell mEPSCs. We defined events within one SD of the mean of the first peak to be "uniquantal" and considered larger events to be "multiquantal." Multiquantal release events accounted for 34.1 ± 4% of all $I_{A(glu)}$ events (n = 7) and, because some events are quite large, made up an even larger fraction of the total spontaneous glutamate release from rods (42.7 ± 8%; n = 7).

We compared pre- and postsynaptic measurements of glutamate release at the same synapses by obtaining simultaneous whole cell recordings from rods and a postsynaptic horizontal cell. Both the rod and its postsynaptic partner horizontal cell were voltage clamped at hyperpolarized potentials as follows: −70 (−75 mV after correcting for LJP) and −60 mV (−72 mV after LJP correction), respectively. We confirmed that these neurons were synaptically connected by determining whether an EPSC could be evoked in the horizontal cell by a strong depolarizing step applied to the rod. We then recorded a long series of spontaneous $I_{A(glu)}$ events in the rod and mEPSCs in the horizontal cell (Fig. 2 *A*). Spontaneous mEPSCs in horizontal cells were faster than $I_{A(glu)}$ events in rods (Fig. 2 *B*). mEPSCs averaged 10.39 ± 0.79 pA (n = 8 cells, n = 451–1715 events/cell) in amplitude with an average rise time of 1.44 ± 0.21 ms, half width of 3.52 ± 0.71 ms, and decay time of 4.30 ± 0.39 ms.

Occasionally, a presynaptic $I_{A(glu)}$ event occurred at the same time as an mEPSC in the horizontal cell. Most pre- and postsynaptic events were not correlated because of the following: 1) many mEPSCs in the horizontal cell arise from release by photoreceptors other than the voltage-clamped rod, and 2) only a few of the roughly seven ribbons per rod contact any individual horizontal cell (6,58). Despite the low frequency of correlated events, the cross correlation between long segments of baseline currents recorded from synaptically coupled rods and horizontal cells (R^2 = 0.32 ± 0.076, n = 8 pairs) was significantly greater than the cross correlation observed after time shifting the horizontal cell current record by 100 ms (R^2 = 0.08 ± 0.017; $p = 0.025$, paired t-test).

We examined individual rod $I_{A(glu)}$ and horizontal cell mEPSCs in which the peak of the $I_{A(glu)}$ event occurred 10 ms or less after onset of an mEPSC. Among such coincident events, the amplitude of $I_{A(glu)}$ events and mEPSCs were linearly correlated (R^2 = 0.36, Table 1) and showed a significant nonzero slope in 6/8 pairs ($p < 0.05$, Fig. 2 *C*; Table 1). Because of the high frequency of spontaneous mEPSCs, a few coincident events can occur by chance. However, the correlation of amplitudes between coincident pre- and postsynaptic events was abolished by time shifting the records (R^2 = 0.02), and 0/8 pairs showed slopes that were significantly nonzero.

Glutamate molecules bind rapidly to EAAT glutamate transporters, and this binding activates $I_{A(glu)}$. The cycle time for glutamate transporter is rather slow, ∼70 ms (59), so the increase in $I_{A(glu)}$ during a pulse of glutamate effectively integrates presynaptic glutamate release (60). Differentiating the glutamate transporter current should therefore provide a measure of the rise in synaptic glutamate levels. Consistent with this, differentiating the glutamate

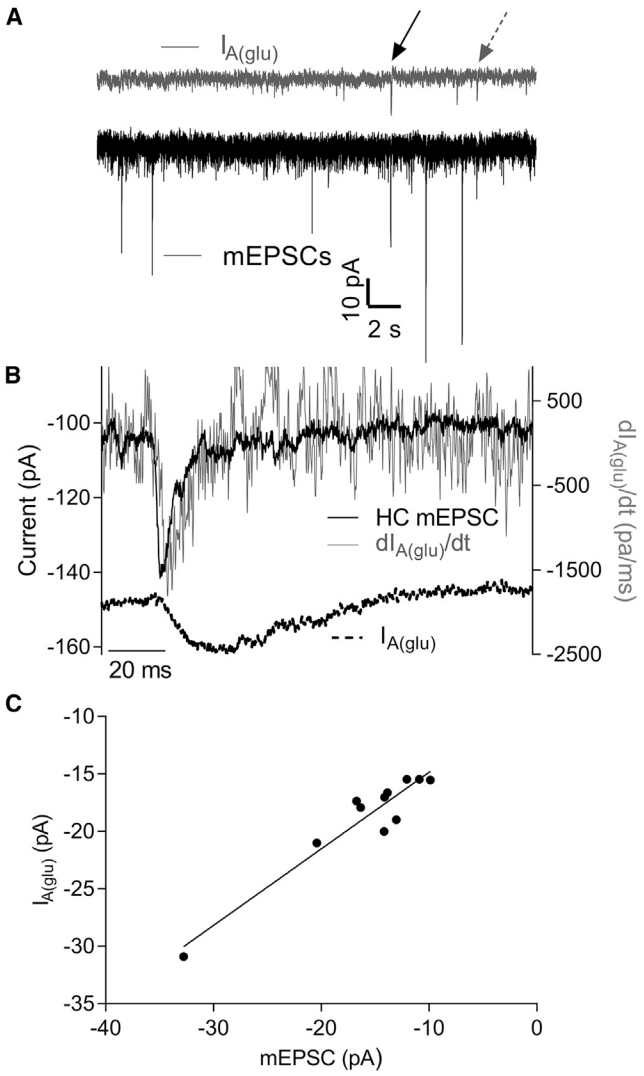

FIGURE 2 Simultaneous recordings of spontaneous $I_{A(glu)}$ events in a rod and miniature EPSCs (mEPSCs) in a horizontal cell. (*A*) During this record, two spontaneous presynaptic $I_{A(glu)}$ multiquantal events in rods (*upper gray trace*) occurred simultaneously (*arrows*) with postsynaptic mEPSCs (*lower black trace*). (*B*) Coincident mEPSC (*upper black trace*) and presynaptic $I_{A(glu)}$ (*lower black trace*) events (*A*, *dashed gray arrow*) are shown. The noise gray trace shows the first derivative of $I_{A(glu)}$. The close match between the derivative of $I_{A(glu)}$ and mEPSC time course indicates that the increase in $I_{A(glu)}$ integrates glutamate release from the rod. (*C*) The amplitudes of coincident pre- and postsynaptic events were linearly correlated ($n = 11$, $R^2 = 0.9$) with a slope that was significantly nonzero (F-test, $p < 0.001$), demonstrating that $I_{A(glu)}$ provides a presynaptic measure of glutamate release.

transporter currents from individual large $I_{A(glu)}$ events yielded waveforms with kinetics that closely matched the kinetics of simultaneously recorded mEPSCs that reflect glutamate binding to α-amino-3-hydroxy-5-methyl-4-isoxazolepropionic acid receptors on horizontal cells (Fig. 2 *B*). In these recordings, the latency to the peak of mEPSCs was attained at 3.13 ± 0.19 ms, and the peak of the differentiated $I_{A(glu)}$ occurred 2.0 ± 0.38 ms later ($n = 8$ events). Assuming a diffusion coefficient for glutamate of 0.33 μm/s (61), a total latency of 5.1 ms places an upper limit to the average distance between release sites and glutamate transporters of 3.37 μm. The correlated amplitude and kinetic properties of coincident pre- and postsynaptic events in paired recordings indicates that $I_{A(glu)}$ provides a dependable presynaptic measure of glutamate release.

The kinetics of large, multiquantal $I_{A(glu)}$ events matched those of small events. Fig. 3 *A* shows the average of small ($n = 97$) and large ($n = 20$) $I_{A(glu)}$ events from a single rod (selected by a template with defined amplitude parameters). After scaling the average small uniquantal event to match the large multiquantal average, the time courses of the two closely matched one another (*red trace*, Fig. 3 *A*). The 10–90% rise time did not differ significantly between uniquantal and multiquantal events ($p = 0.72$; Mann-Whitney test), and the rise time was not correlated with event amplitude (Fig. 3 *B*). The variance among 10–90% rise times was greater for small events because baseline noise more often hindered the accurate detection of start and stop times with smaller events. These data suggest that large and small events result from kinetically similar mechanisms.

We also compared the kinetics of large and small mEPSCs. Fig. 3 *C* shows an example of average large and small mEPSCs from the same horizontal cell. After scaling the small event to match the amplitude of the large event (*red trace*, Fig. 3 *C*), the rise times of the two waveforms closely matched one another. Uniquantal and multiquantal EPSC 10–90% rise times were 1.42 ± 0.01 vs. 1.43 ± 0.03 ms, respectively, and did not differ significantly ($p = 0.25$, $n = 9$ cells). In this example, the average large event decayed more slowly than the average uniquantal event, consistent with a greater persistence of glutamate in the cleft after the release of multiple vesicles. However, because of variability among half-width measurements, the overall difference in half widths between uniquantal and multiquantal mEPSCs was not statistically significant across the entire sample ($p = 0.18$, $n = 9$ cells). The similar rise times for large and small events suggests that large events arise from the closely synchronized release of multiple vesicles.

Comparing evoked and spontaneous release

We compared the amplitude of spontaneous $I_{A(glu)}$ events to $I_{A(glu)}$ evoked by 2-ms depolarizing pulses to −25 mV. For these experiments, we alternated recordings of spontaneous and evoked events, waiting at least 45 s between test pulses for replenishment of the releasable pool of vesicles. Evoked release ran down during our recordings, and so for this analysis, we only included recordings in which evoked release persisted long enough for us to measure at least 10 trials. We constructed amplitude histograms for both spontaneous and evoked events. The example in Fig. 4 shows a recording in which the evoked amplitude appears quantized. When fit with multiple Gaussians, the average fundamental

TABLE 1 Descriptions of Coincident Pre- and Postsynaptic Events, Including the Number of Coincident Events (*n*) from Paired Rod and Horizontal Cell Recordings

Pair	*n*	Slope	R^2	*p* (F-test)	Rod QA (pA)	Rod CV	HC QA (pA)	HC CV
1	39	0.47 ± 0.08	0.49	<0.0001	5.5	0.09	8.6 ± 1.7	0.20
2	43	1.40 ± 0.35	0.28	0.0003	5.7	0.11	9.5 ± 2.1	0.22
3	34	2.10 ± 0.60	0.28	0.0014	6.9	0.12	7.6 ± 1.3	0.17
4	24	2.12 ± 0.90	0.19	0.03	7.8	0.09	15.2 ± 0.6	0.04
5	34	0.14 ± 0.16	0.02	0.39	6.3	0.10	3.6 ± 0.3	0.08
6	12	0.47 ± 0.21	0.33	0.05	7.8	0.04	15.7 ± 1.3	0.08
7	35	0.62 ± 0.13	0.4	<0.0001	10.8	0.08	15.3 ± 0.5	0.03
8	11	0.66 ± 0.07	0.9	<0.0001	12.4	0.14	16.5 ± 0.9	0.05
mean	29	1.00	0.36	0.09	7.9	0.09	11.5	0.1
σ	12.1	0.77	0.26	0.17	2.5	–	–	–

Regression statistics are reported from amplitudes of coincident events plotted against one another. Events were considered coincident if the start of the rod event occurred within 10 ms of the peak of horizontal cell (HC) mEPSC. Six out of eight pairs show a slope that deviated significantly from zero (F-test). Rod and HC quantal amplitudes (QA) are reported, along with a coefficient of variance (CV).

amplitude did not differ between evoked and spontaneous events ($p = 0.29$; $n = 4$, paired *t*-test), consistent with the hypothesis that the first peak in the amplitude histogram reflects the release of a single vesicle, and subsequent peaks reflect release of multiple vesicles (Fig. 4 *B*).

Spontaneous and evoked release appear to access different vesicle pools. In some trials, we tested release using a short, strong test pulse (2 ms, −70 to −10 mV) to maximally activate I_{Ca} but avoid stimulating Ca^{2+}-activated Cl^- currents. In these experiments, we alternated 3-min recordings of spontaneous activity with 2-ms test pulses to −10 mV. This depolarizing stimulus depletes a large fraction of the readily releasable pool of available vesicles. The readily releasable pool in rods averages 25 vesicles/ribbon, matching the number of vesicles that contact the plasma membrane at the base of a rod ribbon (62), and there are an average of seven ribbons per salamander rod (6,55,58), suggesting a total readily releasable pool of ~175 vesicles/rod. Rod ribbons are typically separated from one another by 1 μm or more (55,58,63), so it is unlikely that vesicles at neighboring ribbons would spontaneously fuse together. Although spontaneous events presumably arise from individual ribbons, whereas evoked responses reflect release from all of the functional ribbons, spontaneous events often exceeded evoked responses in the same cell. In 12/18 rods, at least one spontaneous event exceeded the amplitude of the largest evoked response in that cell. An example of large spontaneous events recorded before and after a smaller evoked response are shown in Fig. 5 *A*. The largest evoked response averaged 73.7 ± 12.3 pA ($n = 18$ rods), whereas the largest spontaneous event recorded in the same cells averaged 92.9 ± 13.2 pA. If the entire readily releasable pool of 25 vesicles/ribbon were available for release from all of the ribbons in a rod, then we should have seen much larger evoked responses. This suggests that there was considerable rundown of the evoked response even before the first test pulse was applied (at least 3 min after patch rupture), but nevertheless, rods remained capable of large spontaneous responses.

We saw no evidence for cross-depletion between spontaneous and evoked release. In Fig. 5 *B*, we plot the ratio of the amplitude of spontaneous multiquantal events relative to the amplitude of the evoked response as a function of time before (open circles) or after (filled circles) a test pulse applied at time 0. For this analysis, we only included events in which both spontaneous and evoked events were at least 30 pA in amplitude. The amplitude of spontaneous events relative to evoked events did not vary in any systematic way with time of occurrence relative to the evoked response. Consistent with this, the slope of linear regressions fit to the data for spontaneous events occurring before or after the test pulse did not differ significantly from zero ($p = 0.58$ after test pulse; $p = 0.77$ before test pulse). These data suggest that the amplitude of a prior evoked response did not significantly influence the amplitude of a subsequent spontaneous event and vice versa (Fig. 5 *B*).

For the analysis in Fig. 5 *B*, we required that both evoked and spontaneous responses exceed 30 pA. However, as illustrated in Fig. 5 *C*, we often saw cases in which the depolarizing test pulse failed to evoke any release whatsoever, but a large spontaneous event was nevertheless observed in the same cell. By showing that spontaneous multiquantal release does not require that evoked release from ribbons remain intact, this illustrates an extreme case of the absence of cross-depletion. The rapid rundown of evoked release and the absence of cross-depletion suggest that spontaneous multivesicular and evoked release involve different vesicle pools.

Multiquantal release involves release sites close to Ca^{2+} channels

To determine the dependence of multiquantal $I_{A(glu)}$ events on intracellular Ca^{2+}, we varied the Ca^{2+} buffering capacity of the intracellular solution introduced into rods through the whole cell recording pipette. To localize Ca^{2+} signaling events relative to the source of Ca^{2+}, we exploited differences in the kinetics with which EGTA and BAPTA chelate

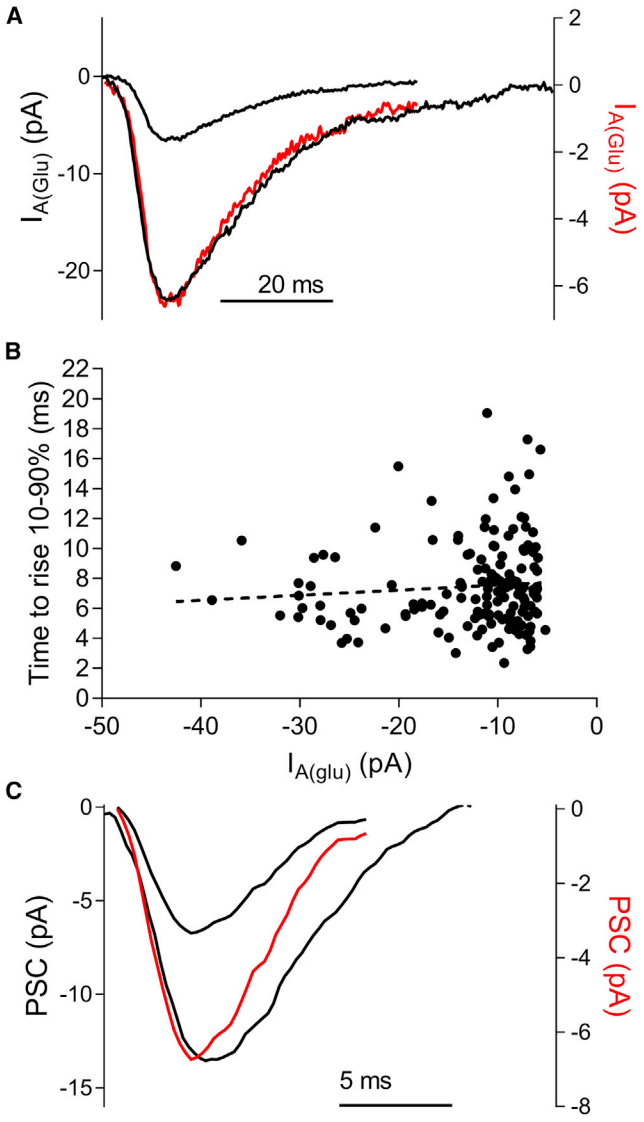

FIGURE 3 Large and small spontaneous release events show similar kinetics. (*A*) Average uniquantal (*small black trace*; $n = 97$) and multiquantal $I_{A(glu)}$ events (*large black trace*; $n = 20$) from a single rod are shown. There were no kinetic differences between the two after scaling the average uniquantal event (*red trace*, *right axis*) to match the amplitude of the average multiquantal event. (*B*) Graph of individual $I_{A(glu)}$ event amplitudes plotted against 10–90% time to rise. The slope of the linear regression (*dotted line*) did not differ significantly from zero (F-test; $p = 0.28$). (*C*) Average uniquantal mEPSC (*small black trace*, $n = 38$) and multiquantal mEPSC ($n = 16$) from a single horizontal cell are shown. Scaling the uniquantal event (*red trace*, *right axis*) to match the amplitude of the larger event revealed that rise times of the two events were equivalent.

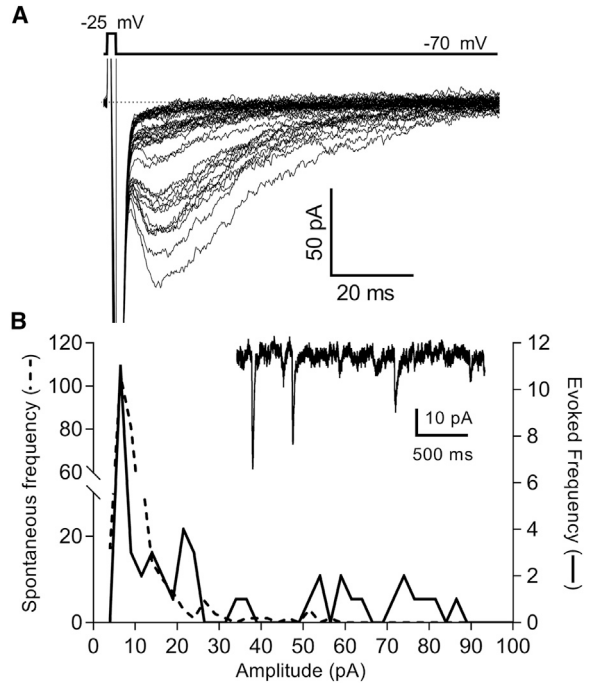

FIGURE 4 Comparisons of evoked and spontaneous $I_{A(glu)}$ events support the interpretation that the first peak in the amplitude histogram of spontaneous release events reflects the release of a single vesicle, and subsequent peaks reflect the release of multiple vesicles. (*A*) A series of 41 overlaid $I_{A(glu)}$ responses evoked by 2-ms steps to −25 mV in a rod are shown. Peak amplitudes of these evoked responses are plotted in the amplitude histogram in (*B*) (*solid line*). The amplitudes of spontaneous $I_{A(glu)}$ events from the same rod were also plotted in (*B*) (*dashed line*), revealing a similar fundamental uniquantal amplitude ($n = 289$ events). The inset in (*B*) shows an example of spontaneous events from this same cell.

Ca^{2+}. Although both chelators have the same affinity, the slower buffer EGTA will have less of an effect on Ca^{2+} levels near the source than the faster buffer BAPTA. The graph in Fig. 6 *A* plots Ca^{2+} levels as a function of distance from an open Ca^{2+} channel as predicted by an Excel-based macro, "Pore" (64). The graph predicts that Ca^{2+} levels will decline to 100 nM within 100 nm of an open Ca^{2+} channel when the patch pipette solution is buffered with 10 mM BAPTA. With 5 mM EGTA, Ca^{2+} levels are predicted to stay above 1 μM for 390 nm from a channel. Lowering Ca^{2+} buffering to 0.05 mM, which approximates endogenous buffering in salamander rods (65), allows Ca^{2+} to remain above 1 μM for almost 780 nm from an open channel.

The frequency of uniquantal events was reduced by limiting the spread of Ca^{2+} with 5 mM EGTA compared with 0.05 mM EGTA and further reduced by using 10 mM BAPTA as the chelator (Fig. 6 *B*, $p < 0.0001$; one-way analysis of variance (ANOVA)/Tukey's multiple comparisons). This suggests that some uniquantal events occur well outside of Ca^{2+} nanodomains generated by Ca^{2+} sources, consistent with imaging results showing that many spontaneous release events in rods occur at nonribbon release sites (11). By contrast, the frequency of multiquantal events did not differ between 5 and 0.05 mM EGTA and was only reduced by 10 mM BAPTA (Fig. 6 *C*). This suggests that multiquantal release involves vesicles within a few hundred nanometers of Ca^{2+} channels that are in turn situated just beneath ribbons (66–69).

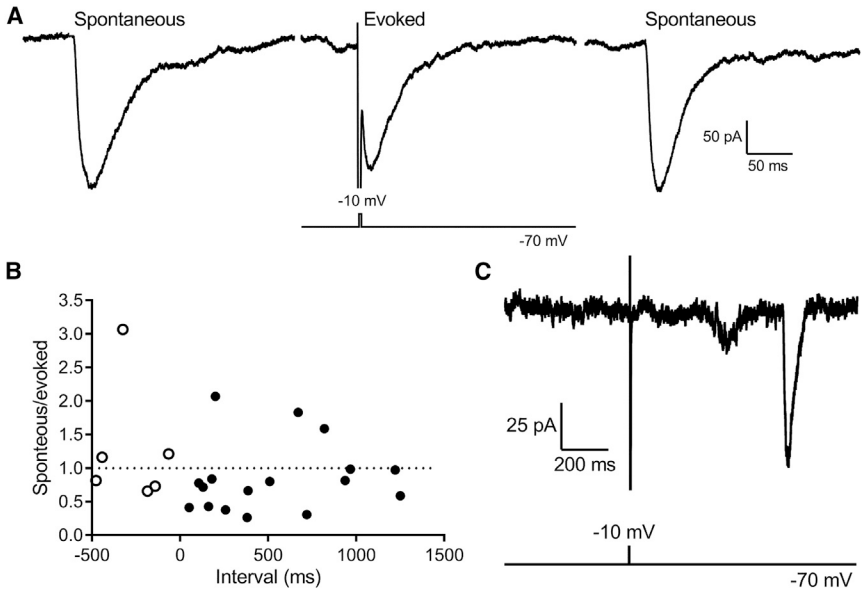

FIGURE 5 Large spontaneous events involve a different vesicle pool than evoked release. (*A*) Shown are examples of spontaneous events that occurred before and after a smaller event evoked by a depolarizing step to −10 mV (2 ms). (*B*) Ratio of the amplitude of spontaneous multiquantal events relative to an evoked response in the same trial is shown. These ratios are plotted as a function of the timing of the spontaneous event before (*open circles*) or after (*filled circles*) the test stimulus (2 ms, −10 mV) applied at time 0. Spontaneous and multiquantal events were included in this analysis only if both exceeded 30 pA. Data were from 1-s ($n = 5$) and 2-s ($n = 18$) trials. (*C*) Shown is an example of a large spontaneous multiquantal event that occurred 650 ms after a depolarizing pulse (2 ms to 10 mV) failed to evoke release.

A previous study suggested that the activation of Ca^{2+}-induced Ca^{2+} release (CICR) in rods can increase coordinated vesicle release (17). We tested contributions of CICR during spontaneous release by bath applying a ryanodine receptor inhibitor, dantrolene (10 μM), but did not see any significant change in the frequency of spontaneous multiquantal release when compared with vehicle control ($p = 0.98$; two-way ANOVA).

Multiquantal events originate on the ribbon

The Ca^{2+} chelator results suggest that multiquantal release involves release sites close to Ca^{2+} channels beneath synaptic ribbons. As a more direct test of whether multiquantal release involves ribbon release sites, we damaged the ribbon by FALI with a FITC-RIBEYE-binding peptide. As a control, we used a FITC-conjugated scrambled version of the same peptide. We introduced the peptides through a patch pipette. As illustrated in Fig. 7 *A*, the FITC-RIBEYE-binding peptide binds selectively to ribbons, yielding bright spots (arrow) in the synaptic terminal when imaged with a confocal microscope. The pipette solutions included the antioxidants trolox (3 mM) and reduced glutathione (3 mM) to limit nonspecific oxidative damage. We waited 5 min to allow time for the peptide to enter the cell and then turned on a 488-nm laser for 60 s to bleach the dye. Bleaching of FITC by FALI releases singlet oxygen that causes damage localized to within 50 Å of the FITC moiety (70).

Fast synchronous, evoked release from rods is largely ribbon dependent (6,71,72), and so, a short depolarizing step should evoke release almost exclusively from ribbon-associated vesicles. Consistent with this, $I_{A(glu)}$ evoked by a 2-ms depolarizing step to −10 mV was nearly abolished after damaging the ribbon by FALI (*filled squares* and insets, Fig. 7 *B*). When using the scrambled peptide, evoked release ran down over time but was not abolished acutely by the laser (*open squares*, Fig. 7 *B*). Laser inactivation with FITC-RIBEYE also reduced the frequency of spontaneous multiquantal events (*filled squares*, Fig. 7 *C*) compared with control (*open squares*, $p = 0.03$) but did not significantly affect the frequency of uniquantal events (Fig. 7 *D*, $p = 0.97$). The few multiquantal events that remain after FALI may reflect incomplete damage to the ribbon as found earlier with this same peptide concentration (73). These results extend those seen with Ca^{2+} buffering by revealing that multiquantal release depends on the presence of functional synaptic ribbons.

Multiquantal release involves syntaxin 3B

Studies at ribbon synapses and in non-neuronal secretory cells have both suggested a role for syntaxin 3 in supporting intervesicular SNARE complexes and vesicle-vesicle fusion (23,27). To test whether syntaxin 3B is involved in multiquantal release from rods, we introduced a short peptide based upon the N-terminal region of the SNARE domain of syntaxin 3B (stx3pep) or a scrambled version of this peptide (control) into rods through a patch pipette. The stx3pep has been shown to inhibit the formation of SNARE complexes in retinal ribbon synapses (18). The frequency of all events, tallied in 3-min bins, ran down over time during recordings with both peptides, but the stx3pep inhibitory peptide caused a significantly greater reduction in the frequency of multiquantal events over time compared with the control peptide (Fig. 8, $p < 0.007$, two-way ANOVA). By contrast, there was no change in the frequency of uniquantal events with stx3pep compared with the scrambled control peptide after 15 min (Fig. 8, $p = 0.94$, unpaired

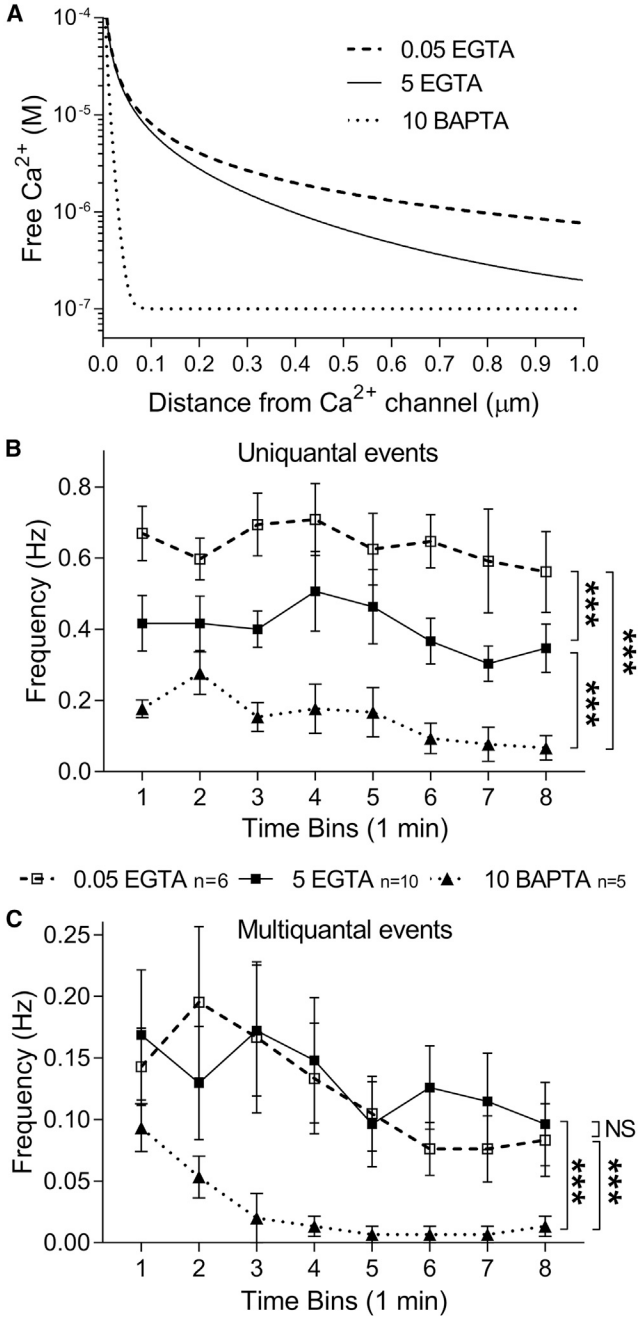

FIGURE 6 Effects of Ca^{2+} chelators on spontaneous release indicate that multiquantal release involves vesicles situated close to intracellular Ca^{2+} sources. (*A*) Shown is a graph of intracellular Ca^{2+} levels plotted as a function of distance from an open Ca^{2+} channel, predicted from the Excel-based macro "Pore" (64). (*B*) Shown are the frequencies of uniquantal events from rods plotted as a function of time after obtaining a whole cell recording from a rod with different Ca^{2+} buffers in the patch pipette solution. The frequency of uniquantal events was reduced significantly when buffering was raised from 0.05 (*open squares*, $n = 7$ rods) to 5 mM EGTA (*filled squares*, $n = 10$) and reduced further with 10 mM BAPTA (*triangles*, $n = 5$) as the chelator ($p < 0.0001$; one-way ANOVA/Tukey's multiple comparisons). (*C*) Multiquantal event frequency did not differ between 0.05 and 5 mM EGTA but was reduced significantly by 10 mM BAPTA ($p < 0.0001$; one-way ANOVA/Tukey's multiple comparisons). Data points show mean ± SEM.

t-test). These results suggest that multiquantal events are SNARE mediated and are preferentially affected by acute perturbation of syntaxin 3B function.

DISCUSSION

Our results show that multiquantal release occurs frequently in rods, constituting ~30% of spontaneous release events and 40% of the total spontaneous glutamate release. The identical rise times for large versus small $I_{A(glu)}$ events in rods and for large versus small horizontal cell mEPSCs suggest that spontaneous multiquantal release involves synchronous, not sequential, fusion of vesicles. Experiments with exogenous Ca^{2+} buffers showed that synchronous multiquantal release occurs at sites within a few hundred nanometers of Ca^{2+} channels that are in turn close to ribbons in rod terminals. Selectively damaging ribbons by FALI and interfering with syntaxin 3B by the use of an inhibitory peptide both reduced multiquantal but not uniquantal events. Together, these results are consistent with the hypothesis that simultaneous multiquantal release from rods arises from homotypic fusion among neighboring vesicles on a ribbon and involves the SNARE protein, syntaxin 3B (18). We consider this hypothesis further below.

In hair cells, there is evidence that the spread of Ca^{2+} entering Ca^{2+} channels beneath the ribbon can reach multiple vesicles and thereby facilitate simultaneous multivesicular release (15). By contrast, measurements of release from rods found that a single Ca^{2+} channel opening triggers an average of only 0.17 ± 0.12 (SD) vesicle fusion events—far fewer than needed to account for the frequency of spontaneous multiquantal events observed in rods (6). In rods, it has also been suggested that the amplification of Ca^{2+} influx by CICR might facilitate coordinated multivesicular release (17). We did not observe a significant effect of the CICR blocker dantrolene on spontaneous multiquantal release, although CICR may play a bigger role in amplifying release during evoked release at more depolarized potentials (17). Still, consistent with an earlier study on spontaneous release from rods (11), our results with BAPTA show that the frequency of multiquantal events depends strongly on available $[Ca^{2+}]_i$. This is similar to the finding at ribbon synapses of bullfrog hair cells that 10 mM BAPTA almost completely abolishes release events (2). The most likely source for Ca^{2+} ions to support spontaneous release is the stochastic opening of L-type Ca^{2+} channels clustered beneath ribbons. Consistent with this, deletion of RIM1/2 or RIM-binding proteins from ribbon synapses caused a reduction in Ca^{2+} influx through L-type Ca^{2+} channels along with a reduction in spontaneous release (74,75). By contrast to the apparent Ca^{2+} dependence of spontaneous release at ribbon synapses, spontaneous release at many conventional excitatory synapses depends less on Ca^{2+} entry from voltage-gated channels than does spontaneous release at inhibitory synapses (76–81). It is hypothesized that these differences in

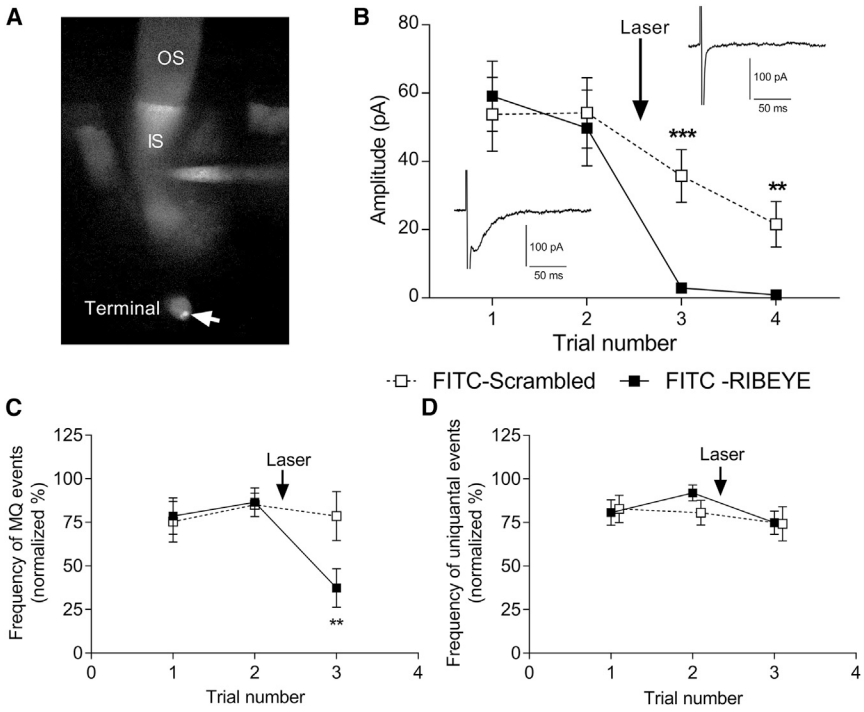

FIGURE 7 Fluorophore-assisted laser inactivation (FALI) of ribbons with a FITC-conjugated RIBEYE-binding peptide indicates that multiquantal release occurs preferentially at ribbon release sites. (*A*) Confocal *z*-stack image of a rod after introducing the peptide through a patch pipette is shown. Weak fluorescence from cytoplasmic dye is visible in the outer segment (OS) and inner segment (IS). Two small bright spots in the terminal (*arrow*) show dye bound to ribbons before laser bleaching. (*B*) Damaging ribbons by FALI reduced evoked $I_{A(glu)}$ events evoked by a brief depolarizing stimulus (2 ms, −25 mV). The insets show examples of responses evoked in a rod before and after 60-s bleach with 488-nm laser light. (*C*) FALI with the RIBEYE-binding peptide significantly reduced the frequency of multiquantal events ($n = 7$ rods; $p = 0.0127$; two-way ANOVA/Tukey's multiple comparisons), but FALI with a scrambled control peptide did not ($n = 7$, $p = 0.91$; two-way ANOVA/Tukey's multiple comparisons). (*D*) FALI did not reduce the frequency of uniquantal events with either the RIBEYE-binding ($p = 0.3$; 2-way ANOVA/Tukey's multiple comparisons) or scrambled control peptide ($p = 0.84$; 2-way ANOVA/Tukey's multiple comparisons). Data points show mean ± SEM.

spontaneous release at conventional excitatory and inhibitory synapses arise from differences in the protein isoforms used by those synapses (77). Similarly, the greater dependence of spontaneous glutamate release on voltage-gated Ca^{2+} channels at ribbon synapses may reflect a reliance on particular protein isoforms. For example, as we consider below, the Ca^{2+} dependence in multiquantal release might involve actions of Ca^{2+} or Ca^{2+}/calmodulin-dependent protein kinase II (CaMKII) on syntaxin 3B, a target SNARE protein specific to retinal ribbon synapses, that occur before final fusion.

Could the heterogeneous amplitudes of $I_{A(glu)}$ be due to a variable dilation of fusion pores rather than multiquantal release, as proposed for inner hair cells (10)? We found that large and small events showed matching kinetics, as found in bullfrog hair cells (2), and rarely saw multiphasic events that are commonly seen in inner hair cells from rats. Multiphasic events at rat hair cell synapses are thought to reflect fusion pore flickering and thus show similar charge transfer for both large and small events (10). However, we found that event amplitude and charge transfer increased in parallel with one another, indicating that larger events result from a greater release of glutamate (10,57). This suggests that the variability in amplitude of release events in rods is unlikely to arise from flickering openings of the fusion pore.

Our results show a role for both ribbons and syntaxin 3B in facilitating synchronous multiquantal release. Consistent with these results, genetic deletion of syntaxin 3 reduced multiquantal but not uniquantal release frequency in peritoneal mast cells (24). One way in which syntaxin 3B might facilitate multivesicular release would be to promote homotypic fusion among vesicles. Consistent with the ability of vesicles to fuse with one another on the ribbon, repetitive stimulation led to an enlargement of ribbon-attached cisternae in retinal bipolar cells (29). Although most syntaxin 3B is located on the plasma membrane, it can also be found on vesicular membranes at ribbon synapses, in which it could potentially form SNARE complexes with vesicle SNAREs on neighboring vesicles (44). The proximity of neighboring vesicles on the ribbon and their situation near Ca^{2+} channels would facilitate vesicle-vesicle interactions (18).

We observed that spontaneous multiquantal release could occur in rods that are no longer capable of evoked release because of rundown. The ability for spontaneous release to occur in the absence of evoked release is consistent with evidence from rods and other neurons that spontaneous and evoked pools show functional and molecular differences (11,82,83). Although they involve different pools, FALI experiments showed that evoked and spontaneous multiquantal release both occur at ribbons. The differing capabilities for Ca^{2+}-dependent and -independent release may reflect differences in the composition of the SNARE complexes among different ribbon-associated vesicles (83).

The rundown of evoked release is not due to rundown of $I_{Ca,}$ which remains stable for long periods of recording from salamander rods (data not shown). Instead, the loss of evoked release is likely due to impairment of the Ca^{2+}-dependent fusion apparatus. This interpretation is in line

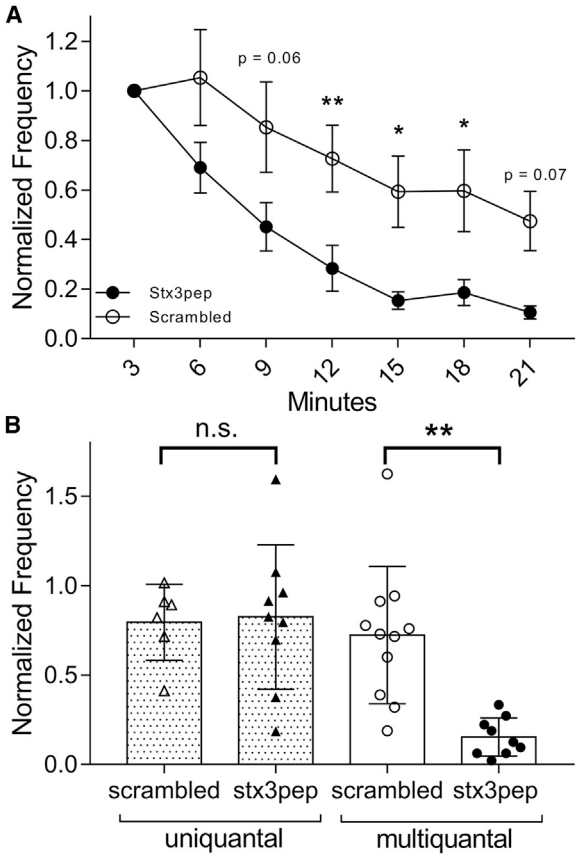

FIGURE 8 Inhibiting the SNARE protein syntaxin 3B by introducing an inhibitory peptide (stx3pep) into a rod through the patch pipette selectively reduced multiquantal but not uniquantal release. (*A*) Spontaneous multiquantal event frequency measured in 3-min bins after beginning the whole cell recording was reduced by stx3pep ($n = 12$) compared with a scrambled control peptide ($n = 9$, $p = 0.002$; two-way ANOVA). Data points show mean ± SEM. (*B*) Comparison of uniquantal and multiquantal event frequency measured 15 min after patch rupture is shown. The frequency of uniquantal events did not differ between stx3pep (*filled triangles*) and scrambled control peptide (*open triangles*), but the frequency of multiquantal events was reduced significantly by stx3pep (*filled circles*) relative to the scrambled control peptide (*open circles*, $p < 0.003$; one-way ANOVA, Tukey's multiple comparisons). Bars show mean ± SD.

with previous evidence indicating that the final fusion step for spontaneous multiquantal release in rods does not necessarily require Ca^{2+} (11) and thus should be less affected, as observed. That spontaneous multivesicular release can occur without being triggered by stimulus-evoked Ca^{2+} entry also argues against the idea that the spontaneous release of multiple vesicles is coordinated by the spread of Ca^{2+} beneath the ribbon or by sequential Ca^{2+}-dependent fusion of vesicles further up the ribbon. A more likely explanation for spontaneous multivesicular release is prior homotypic fusion among vesicles.

Although the final fusion step during spontaneous multiquantal release can occur in a Ca^{2+}-independent manner, our results also showed a dependence of multiquantal release on Ca^{2+} levels near the ribbon. This may reflect the actions of Ca^{2+} during the delivery and priming of vesicles on the ribbon. CaMKII is located on ribbons (84,85), and the activation of this enzyme facilitates the open configuration of syntaxin 3B, enhancing its interactions with SNAP-25 (44). Prior elevation of cytoplasmic Ca^{2+} acting on CaMKII localized to ribbons could thus promote homotypic fusion between neighboring vesicles on the ribbon, explaining the preferential reduction of ribbon-mediated multiquantal fusion events by the inhibitory peptide, stx3pep.

The functional role of multiquantal release at this synapse is not entirely clear. Although variability in the amplitude of spontaneous release events might be expected to impair detection of small light-evoked changes in release, the ability to coordinate fusion of multiple vesicles during evoked release could improve the coding for contrast changes, especially when photoreceptors depolarize in response to light decrements. Multiquantal release might provide a thresholding mechanism at the rod synapse for selectively transmitting large events. Such a mechanism can reduce the impact of noise, although in salamander retina, this type of nonlinearity is thought to be more prominent at bipolar cell synapses (86). A recent study concluded that multivesicular release at bipolar cell ribbon synapses improves temporal precision for detecting contrast changes and showed that a single vesicle provides more information about the preceding stimulus change during multivesicular release than during univesicular release (14).

AUTHOR CONTRIBUTIONS

W.B.T., C.L.H., and R.H. conceived and planned the project. R.H. and R.J. provided stx3pep and scrambled peptides. C.L.H., J.J.G., and X.W. performed experiments. C.L.H. and W.B.T. analyzed data. Manuscript was written by C.L.H., W.B.T., and R.H.

ACKNOWLEDGMENTS

Supported by National Institutes of Health grants EY10542 (W.B.T.), EY28848 (J.J.G.), and EY012128 (R.H.), Research to Prevent Blindness Senior Scientific Investigator Award (W.B.T.), and the Frederic B. Asche Foundation (R.H.).

REFERENCES

1. Rudolph, S., M. C. Tsai, …, J. I. Wadiche. 2015. The ubiquitous nature of multivesicular release. *Trends Neurosci.* 38:428–438.
2. Li, G. L., E. Keen, …, H. von Gersdorff. 2009. The unitary event underlying multiquantal EPSCs at a hair cell's ribbon synapse. *J. Neurosci.* 29:7558–7568.
3. Brandt, A., D. Khimich, and T. Moser. 2005. Few CaV1.3 channels regulate the exocytosis of a synaptic vesicle at the hair cell ribbon synapse. *J. Neurosci.* 25:11577–11585.
4. Jarsky, T., M. Tian, and J. H. Singer. 2010. Nanodomain control of exocytosis is responsible for the signaling capability of a retinal ribbon synapse. *J. Neurosci.* 30:11885–11895.
5. Bartoletti, T. M., S. L. Jackman, …, W. B. Thoreson. 2011. Release from the cone ribbon synapse under bright light conditions can be

controlled by the opening of only a few Ca(2+) channels. *J. Neurophysiol.* 106:2922–2935.

6. Van Hook, M. J., and W. B. Thoreson. 2015. Weak endogenous Ca2+ buffering supports sustained synaptic transmission by distinct mechanisms in rod and cone photoreceptors in salamander retina. *Physiol. Rep.* 3:e12567.
7. Mennerick, S., and G. Matthews. 1996. Ultrafast exocytosis elicited by calcium current in synaptic terminals of retinal bipolar neurons. *Neuron.* 17:1241–1249.
8. Cadetti, L., D. Tranchina, and W. B. Thoreson. 2005. A comparison of release kinetics and glutamate receptor properties in shaping rod-cone differences in EPSC kinetics in the salamander retina. *J. Physiol.* 569:773–788.
9. Wen, X., G. W. Saltzgaber, and W. B. Thoreson. 2017. Kiss-and-run is a significant contributor to synaptic exocytosis and endocytosis in photoreceptors. *Front. Cell. Neurosci.* 11:286.
10. Chapochnikov, N. M., H. Takago, …, T. Moser. 2014. Uniquantal release through a dynamic fusion pore is a candidate mechanism of hair cell exocytosis. *Neuron.* 83:1389–1403.
11. Cork, K. M., M. J. Van Hook, and W. B. Thoreson. 2016. Mechanisms, pools, and sites of spontaneous vesicle release at synapses of rod and cone photoreceptors. *Eur. J. Neurosci.* 44:2015–2027.
12. Singer, J. H., L. Lassová, …, J. S. Diamond. 2004. Coordinated multivesicular release at a mammalian ribbon synapse. *Nat. Neurosci.* 7:826–833.
13. Grant, L., E. Yi, and E. Glowatzki. 2010. Two modes of release shape the postsynaptic response at the inner hair cell ribbon synapse. *J. Neurosci.* 30:4210–4220.
14. James, B., L. Darnet, …, L. Lagnado. 2019. An amplitude code transmits information at a visual synapse. *Nat. Neurosci.* 22:1140–1147.
15. Graydon, C. W., S. Cho, …, H. von Gersdorff. 2011. Sharp Ca^{2+} nanodomains beneath the ribbon promote highly synchronous multivesicular release at hair cell synapses. *J. Neurosci.* 31:16637–16650.
16. Mehta, B., J. Snellman, …, D. Zenisek. 2013. Synaptic ribbons influence the size and frequency of miniature-like evoked postsynaptic currents. *Neuron.* 77:516–527.
17. Suryanarayanan, A., and M. M. Slaughter. 2006. Synaptic transmission mediated by internal calcium stores in rod photoreceptors. *J. Neurosci.* 26:1759–1766.
18. Datta, P., J. Gilliam, …, R. Heidelberger. 2017. Two pools of vesicles associated with synaptic ribbons are molecularly prepared for release. *Biophys. J.* 113:2281–2298.
19. Parsons, T. D., and P. Sterling. 2003. Synaptic ribbon. Conveyor belt or safety belt? *Neuron.* 37:379–382.
20. Vakilian, M., Y. Tahamtani, and K. Ghaedi. 2019. A review on insulin trafficking and exocytosis. *Gene.* 706:52–61.
21. Messenger, S. W., M. A. Falkowski, and G. E. Groblewski. 2014. Ca^{2+}-regulated secretory granule exocytosis in pancreatic and parotid acinar cells. *Cell Calcium.* 55:369–375.
22. Blank, U. 2011. The mechanisms of exocytosis in mast cells. *Adv. Exp. Med. Biol.* 716:107–122.
23. Eckly, A., J. Y. Rinckel, …, C. Gachet. 2016. Respective contributions of single and compound granule fusion to secretion by activated platelets. *Blood.* 128:2538–2549.
24. Sanchez, E., E. A. Gonzalez, …, R. Adachi. 2019. Syntaxin 3, but not syntaxin 4, is required for mast cell-regulated exocytosis, where it plays a primary role mediating compound exocytosis. *J. Biol. Chem.* 294:3012–3023.
25. Lollike, K., M. Lindau, …, N. Borregaard. 2002. Compound exocytosis of granules in human neutrophils. *J. Leukoc. Biol.* 71:973–980.
26. Alvarez de Toledo, G., and J. M. Fernandez. 1990. Compound versus multigranular exocytosis in peritoneal mast cells. *J. Gen. Physiol.* 95:397–409.
27. Zhu, D., E. Koo, …, H. Y. Gaisano. 2013. Syntaxin-3 regulates newcomer insulin granule exocytosis and compound fusion in pancreatic beta cells. *Diabetologia.* 56:359–369.
28. He, L., L. Xue, …, L. G. Wu. 2009. Compound vesicle fusion increases quantal size and potentiates synaptic transmission. *Nature.* 459:93–97.
29. Matthews, G., and P. Sterling. 2008. Evidence that vesicles undergo compound fusion on the synaptic ribbon. *J. Neurosci.* 28:5403–5411.
30. Vaithianathan, T., D. Henry, …, G. Matthews. 2016. Nanoscale dynamics of synaptic vesicle trafficking and fusion at the presynaptic active zone. *eLife.* 5:e13245.
31. Gutierrez, B. A., M. A. Chavez, …, R. Adachi. 2018. Munc18-2, but not Munc18-1 or Munc18-3, controls compound and single-vesicle-regulated exocytosis in mast cells. *J. Biol. Chem.* 293:7148–7159.
32. Lam, P. P., M. Ohno, …, H. Y. Gaisano. 2013. Munc18b is a major mediator of insulin exocytosis in rat pancreatic β-cells. *Diabetes.* 62:2416–2428.
33. Woo, S. S., D. J. James, and T. F. Martin. 2017. Munc13-4 functions as a Ca^{2+} sensor for homotypic secretory granule fusion to generate endosomal exocytic vacuoles. *Mol. Biol. Cell.* 28:792–808.
34. Rodarte, E. M., M. A. Ramos, …, R. Adachi. 2018. Munc13 proteins control regulated exocytosis in mast cells. *J. Biol. Chem.* 293:345–358.
35. Klein, O., A. Roded, …, R. Sagi-Eisenberg. 2017. Rab5 is critical for SNAP23 regulated granule-granule fusion during compound exocytosis. *Sci. Rep.* 7:15315.
36. Thorn, P., and H. Gaisano. 2012. Molecular control of compound Exocytosis: a key role for VAMP8. *Commun. Integr. Biol.* 5:61–63.
37. Behrendorff, N., S. Dolai, …, P. Thorn. 2011. Vesicle-associated membrane protein 8 (VAMP8) is a SNARE (soluble N-ethylmaleimide-sensitive factor attachment protein receptor) selectively required for sequential granule-to-granule fusion. *J. Biol. Chem.* 286:29627–29634.
38. Hansen, N. J., W. Antonin, and J. M. Edwardson. 1999. Identification of SNAREs involved in regulated exocytosis in the pancreatic acinar cell. *J. Biol. Chem.* 274:22871–22876.
39. Curtis, L. B., B. Doneske, …, R. Janz. 2008. Syntaxin 3b is a t-SNARE specific for ribbon synapses of the retina. *J. Comp. Neurol.* 510:550–559.
40. Curtis, L., P. Datta, …, R. Janz. 2010. Syntaxin 3B is essential for the exocytosis of synaptic vesicles in ribbon synapses of the retina. *Neuroscience.* 166:832–841.
41. Walch-Solimena, C., J. Blasi, …, R. Jahn. 1995. The t-SNAREs syntaxin 1 and SNAP-25 are present on organelles that participate in synaptic vesicle recycling. *J. Cell Biol.* 128:637–645.
42. Yin, P., N. R. Gandasi, …, S. Barg. 2018. Syntaxin clusters at secretory granules in a munc18-bound conformation. *Mol. Biol. Cell.* 29:2700–2708.
43. Borisovska, M. 2018. Syntaxins on granules promote docking of granules via interactions with munc18. *Sci. Rep.* 8:193.
44. Liu, X., R. Heidelberger, and R. Janz. 2014. Phosphorylation of syntaxin 3B by CaMKII regulates the f1ormation of t-SNARE complexes. *Mol. Cell. Neurosci.* 60:53–62.
45. Thoreson, W. B., K. Rabl, …, R. Heidelberger. 2004. A highly Ca2+-sensitive pool of vesicles contributes to linearity at the rod photoreceptor ribbon synapse. *Neuron.* 42:595–605.
46. Arriza, J. L., S. Eliasof, …, S. G. Amara. 1997. Excitatory amino acid transporter 5, a retinal glutamate transporter coupled to a chloride conductance. *Proc. Natl. Acad. Sci. USA.* 94:4155–4160.
47. Eliasof, S., J. L. Arriza, …, M. P. Kavanaugh. 1998. Localization and function of five glutamate transporters cloned from the salamander retina. *Vision Res.* 38:1443–1454.
48. Eliasof, S., J. L. Arriza, …, S. G. Amara. 1998. Excitatory amino acid transporters of the salamander retina: identification, localization, and function. *J. Neurosci.* 18:698–712.
49. Koch, H. P., R. L. Brown, and H. P. Larsson. 2007. The glutamate-activated anion conductance in excitatory amino acid transporters is gated independently by the individual subunits. *J. Neurosci.* 27:2943–2947.

50. Otis, T. S., and C. E. Jahr. 1998. Anion currents and predicted glutamate flux through a neuronal glutamate transporter. *J. Neurosci.* 18:7099–7110.

51. Pulido, C., and A. Marty. 2017. Quantal fluctuations in central mammalian synapses: functional role of vesicular docking sites. *Physiol. Rev.* 97:1403–1430.

52. Van Hook, M. J., and W. B. Thoreson. 2013. Simultaneous whole-cell recordings from photoreceptors and second-order neurons in an amphibian retinal slice preparation. *J. Vis. Exp.* 76:e50007.

53. Zenisek, D., N. K. Horst, …, G. Matthews. 2004. Visualizing synaptic ribbons in the living cell. *J. Neurosci.* 24:9752–9759.

54. Schmitz, F., A. Königstorfer, and T. C. Südhof. 2000. RIBEYE, a component of synaptic ribbons: a protein's journey through evolution provides insight into synaptic ribbon function. *Neuron.* 28:857–872.

55. Pang, J. J., F. Gao, …, S. M. Wu. 2008. How do tonic glutamatergic synapses evade receptor desensitization? *J. Physiol.* 586:2889–2902.

56. Feigenspan, A., and N. Babai. 2015. Functional properties of spontaneous excitatory currents and encoding of light/dark transitions in horizontal cells of the mouse retina. *Eur. J. Neurosci.* 42:2615–2632.

57. Rossi, M. L., M. Martini, …, R. Fesce. 1994. Quantal nature of synaptic transmission at the cytoneural junction in the frog labyrinth. *J. Physiol.* 478:17–35.

58. Townes-Anderson, E., P. R. MacLeish, and E. Raviola. 1985. Rod cells dissociated from mature salamander retina: ultrastructure and uptake of horseradish peroxidase. *J. Cell Biol.* 100:175–188.

59. Wadiche, J. I., J. L. Arriza, …, M. P. Kavanaugh. 1995. Kinetics of a human glutamate transporter. *Neuron.* 14:1019–1027.

60. Szmajda, B. A., and S. H. Devries. 2011. Glutamate spillover between mammalian cone photoreceptors. *J. Neurosci.* 31:13431–13441.

61. Nielsen, T. A., D. A. DiGregorio, and R. A. Silver. 2004. Modulation of glutamate mobility reveals the mechanism underlying slow-rising AMPAR EPSCs and the diffusion coefficient in the synaptic cleft. *Neuron.* 42:757–771.

62. Heidelberger, R., W. B. Thoreson, and P. Witkovsky. 2005. Synaptic transmission at retinal ribbon synapses. *Prog. Retin. Eye Res.* 24:682–720.

63. Lasansky, A. 1978. Contacts between receptors and electrophysiologically identified neurones in the retina of the larval tiger salamander. *J. Physiol.* 285:531–542.

64. Ward, S. M., and J. L. Kenyon. 2000. The spatial relationship between Ca2+ channels and Ca2+-activated channels and the function of Ca2+-buffering in avian sensory neurons. *Cell Calcium.* 28:233–246.

65. Van Hook, M. J., and W. B. Thoreson. 2014. Endogenous calcium buffering at photoreceptor synaptic terminals in salamander retina. *Synapse.* 68:518–528.

66. Nachman-Clewner, M., R. St Jules, and E. Townes-Anderson. 1999. L-type calcium channels in the photoreceptor ribbon synapse: localization and role in plasticity. *J. Comp. Neurol.* 415:1–16.

67. Morgans, C. W. 2001. Localization of the alpha(1F) calcium channel subunit in the rat retina. *Invest. Ophthalmol. Vis. Sci.* 42:2414–2418.

68. tom Dieck, S., W. D. Altrock, …, J. H. Brandstätter. 2005. Molecular dissection of the photoreceptor ribbon synapse: physical interaction of Bassoon and RIBEYE is essential for the assembly of the ribbon complex. *J. Cell Biol.* 168:825–836.

69. Lv, C., T. J. Gould, …, D. Zenisek. 2012. High-resolution optical imaging of zebrafish larval ribbon synapse protein RIBEYE, RIM2, and CaV 1.4 by stimulation emission depletion microscopy. *Microsc. Microanal.* 18:745–752.

70. Hoffman-Kim, D., T. J. Diefenbach, …, D. G. Jay. 2007. Chromophore-assisted laser inactivation. *Methods Cell Biol.* 82:335–354.

71. Chen, M., D. Križaj, and W. B. Thoreson. 2014. Intracellular calcium stores drive slow non-ribbon vesicle release from rod photoreceptors. *Front. Cell. Neurosci.* 8:20.

72. Chen, M., M. J. Van Hook, …, W. B. Thoreson. 2013. Properties of ribbon and non-ribbon release from rod photoreceptors revealed by visualizing individual synaptic vesicles. *J. Neurosci.* 33:2071–2086.

73. Snellman, J., B. Mehta, …, D. Zenisek. 2011. Acute destruction of the synaptic ribbon reveals a role for the ribbon in vesicle priming. *Nat. Neurosci.* 14:1135–1141.

74. Grabner, C. P., M. A. Gandini, …, F. Schmitz. 2015. RIM1/2-mediated facilitation of Cav1.4 channel opening is required for Ca2+-stimulated release in mouse rod photoreceptors. *J. Neurosci.* 35:13133–13147.

75. Luo, F., X. Liu, …, C. Acuna. 2017. Efficient stimulus-secretion coupling at ribbon synapses requires RIM-binding protein tethering of L-type Ca^{2+} channels. *Proc. Natl. Acad. Sci. USA.* 114:E8081–E8090.

76. Williams, C., W. Chen, …, S. M. Smith. 2012. Coactivation of multiple tightly coupled calcium channels triggers spontaneous release of GABA. *Nat. Neurosci.* 15:1195–1197.

77. Tsintsadze, T., C. L. Williams, …, S. M. Smith. 2017. Distinct actions of voltage-activated Ca^{2+} channel block on spontaneous release at excitatory and inhibitory central synapses. *J. Neurosci.* 37:4301–4310.

78. Druzin, M., D. Haage, …, S. Johansson. 2002. Dual and opposing roles of presynaptic Ca2+ influx for spontaneous GABA release from rat medial preoptic nerve terminals. *J. Physiol.* 542:131–146.

79. Liu, H., L. Li, …, Z. Hu. 2018. Spontaneous vesicle fusion is differentially regulated at cholinergic and GABAergic synapses. *Cell Rep.* 22:2334–2345.

80. Scanziani, M., M. Capogna, …, S. M. Thompson. 1992. Presynaptic inhibition of miniature excitatory synaptic currents by baclofen and adenosine in the hippocampus. *Neuron.* 9:919–927.

81. Llano, I., and H. M. Gerschenfeld. 1993. Inhibitory synaptic currents in stellate cells of rat cerebellar slices. *J. Physiol.* 468:177–200.

82. Sara, Y., T. Virmani, …, E. T. Kavalali. 2005. An isolated pool of vesicles recycles at rest and drives spontaneous neurotransmission. *Neuron.* 45:563–573.

83. Crawford, D. C., and E. T. Kavalali. 2015. Molecular underpinnings of synaptic vesicle pool heterogeneity. *Traffic.* 16:338–364.

84. Uthaiah, R. C., and A. J. Hudspeth. 2010. Molecular anatomy of the hair cell's ribbon synapse. *J. Neurosci.* 30:12387–12399.

85. Kantardzhieva, A., M. Peppi, …, W. F. Sewell. 2012. Protein composition of immunoprecipitated synaptic ribbons. *J. Proteome Res.* 11:1163–1174.

86. Chichilnisky, E. J., and F. Rieke. 2005. Detection sensitivity and temporal resolution of visual signals near absolute threshold in the salamander retina. *J. Neurosci.* 25:318–330.